IEEE Access
Multidisciplinary | Rapid Review | Open Access Journal

SPECIAL SECTION ON INTEGRATIVE COMPUTER VISION AND MULTIMEDIA ANALYTICS

Received March 5, 2020, accepted March 21, 2020, date of publication March 24, 2020, date of current version April 9, 2020.

Digital Object Identifier 10.1109/ACCESS.2020.2982910

Image Haze Removal Based on Superpixels and Markov Random Field

YIBO TAN AND GUOYU WANG
College of Information Science and Engineering, Ocean University of China, Qingdao 266100, China
Corresponding author: Yibo Tan (1065858187@qq.com)

This work was supported by the National Natural Science Foundation of China under Grant 61571407.

ABSTRACT Image haze removal is critical for autonomous driving. However, it is a challenging task for the existing image dehazing algorithms to eliminate the block effect completely and handle objects similar to light (such as snowy objects and white buildings). To address this problem, we propose a novel single-image dehazing method based on superpixels and Markov random field. We obtain the transmission map in the superpixel domain to eliminate the block/halo effect and introduce Markov random field to revise the transmission map in the superpixel domain. The key idea is that the sparsely distributed, incorrectly estimated transmittances can be corrected by properly characterizing the spatial dependencies between the incorrectly estimated superpixels and the neighbouring well-estimated superpixels. The experimental results demonstrate that the proposed method outperforms state-of-the-art image dehazing methods.

INDEX TERMS Superpixel, Markov random field, haze removal, edge preservation, dark channel prior.

I. INTRODUCTION

Outdoor images taken in hazy weather have low contrast and visibility. The low image quality will greatly affect human perception of colours in the image and humans' object recognition and matching abilities. There is a broad collection of compelling algorithms for image dehazing, including the multiple image dehazing method [1]–[3], polarization-based methods [4]–[6], and model-based image recovery methods [7]–[14], [15]. Model-based image recovery methods come from physically valid algorithms that remove haze by modelling the optical transmission of imaging in scattering media and the prior information to remove the backscattered light in front of the scene and to compensate for the light attenuation of the scene. Tan [9] proposed a new dehazing method based on Markov random field (MRF) to maximize the local contrast of the image. Although Tan's method can achieve impressive results, the colours of the restored image are usually oversaturated. Fattal [10] proposed an independent component analysis (ICA)-based colour image defogging method; this method is reliable but time consuming. Zhu *et al.* [13] proposed a decay prior for depth estimation, which is transmitted by machine learning. In addition, there are many methods based on image enhancement methods, such as histogram equalization, curvelet transform, homomorphic filtering, wavelet transform, compression sensing [27], [28] and Retinex methods [29], [30], which can increase the overall contrast, make the brightness of the image suitable, and achieve a satisfactory visual effect. However, sometimes the enhanced image seems unreal. One of the well-known methods is He's dark channel prior (DCP) [12], which is recognized as one of the most effective image dehazing methods. However, when the object in the is close to light in colour, the dark channel prior may not be valid. Wang *et al.* [31] proposed a single-image dehazing method based on a physical model and an image brightness component, but this method can easily produce a halo and overexposure effects. Moreover, there have been some other attempts at single-image haze removal [35]–[43].

This paper proposes a new approach for the estimation of the transmittance using a superpixel and MRF model. The dark channel prior is employed to characterize the dependency of the image observation on the transmittance and formulate the energy function in the MRF model. However, the dark channel prior is found for superpixels rather than patches, so the block effect is avoided. However, the problem of the underestimation of the transmittance within the regions where the pixel colours are not dark is inevitable. We assume that the dark channel prior is valid for most of the superpixels of a natural image. With this assumption, the underestimated transmittance in the sparsely distributed regions

The associate editor coordinating the review of this manuscript and approving it for publication was Guitao Cao.

This work is licensed under a Creative Commons Attribution 4.0 License. For more information, see https://creativecommons.org/licenses/by/4.0/

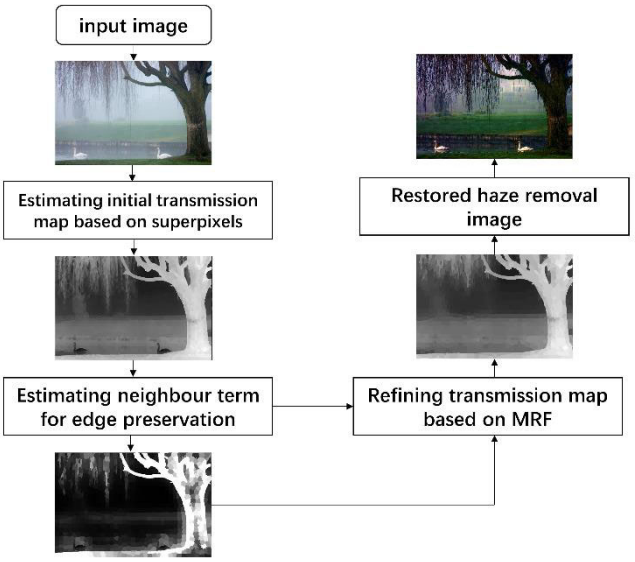

FIGURE 1. The flowchart of the proposed method.

can be properly adjusted by characterizing the smooth term reflecting the spatial dependencies of adjacent superpixels in the MRF model. The flowchart of the proposed method is illustrated in Fig. 1.

II. IMAGE DEHAZING USING SUPERPIXELS AND MRF

A. INITIAL TRANSMISSION MAP ESTIMATION BASED ON the DARK CHANNEL PRIOR AND SUPERPIXELS

The optical model commonly used to describe the image observed in a scattering medium is

$$I(x) = J(x) \cdot t(x) + A \cdot (1 - t(x)) \tag{1}$$

where I is the captured image; J is the scene radiance; A is the pure background light, which is supposed to be available in the image space and is often be evaluated from the image pixels; and t is the medium transmittance. The second term in (1) is the backscattered light in front of the scene. The goal of single-image recovery is to recover J and t from I. Since for each colour channel of the image pixel, both J and t are unknowns in (1); there must be other constraints or priors to solve the underdefined problem. In general, recovery of the scene radiance J relies on the estimation of the transmittance t, which varies at different depths of the scene.

The DCP [12] describes that for a single input image I, the transmittance can be directly estimated by

$$t(x) = 1 - \omega \cdot \min_{y \in \Omega(x)} \left(\min_{c \in \{r,g,b\}} \frac{I^c(y)}{A^c} \right) \tag{2}$$

where $\Omega(x)$ is a patch centred at x, of which the size is generally 15*15 or 11*11 in traditional algorithms; A is the ambient light and ω is a control parameter. However, regardless of the chosen size of $\Omega(x)$, the block effect is inevitable. To handle this problem, He *et al.* s[12] employed a guided filter [26] to refine the transmission map by smoothing the block effect. This method is simple but not very effective,

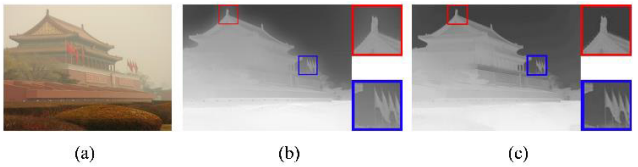

FIGURE 2. (a) Input image. (b-c) Corresponding transmission map obtained by (b) He's method and (c) the proposed method. Red and blue squares are the close-ups of structure's details.

and there are obvious gradually changing artefacts at the edges in the transmission map (Fig. 2(b)). On the other hand, the proposed method successfully preserves the edge details while reducing the artefacts (Fig. 2(c)).

To address this problem, we segment an input image into numerous superpixels by simple linear iterative clustering (SLIC) [16], and we define $\Omega(x)$ as the superpixel to which pixel x belongs. The dark channel can be obtained on the superpixels rather than the traditional patches.

Yang *et al.* [17] and Noh *et al.* [18] calculated the transmittance by using the minimum value of superpixels. However, it is impossible for the boundaries of superpixels to always adhere to the structural edges exactly, which means that a normal minimal operation may also yield a block effect, which is less serious but still evident than that from He's method (Fig. 3). To remove the block effect, we introduce the similarities between the superpixel and its component pixels to successfully select the proper dark channel pixel. Let S_p represent the similarity of pixel p to its belonged superpixel Ω_i. S_p is expressed by the mean vector $\mu_{i,c}$ and the covariance matrix $C_{i,c}$ in RGB colour values (c $\in \{r, g, b\}$). We adopt the probability density function of the multivariate Gaussian distribution to estimate S_p as follows:

$$S_p = \frac{1}{\sqrt{(2\pi)^n \cdot \det(C_{i,c})}} \cdot \exp\left(-\frac{1}{2} \cdot (x_{p,c} - \mu_{i,c})^{\mathrm{T}} \times C_{i,c}^{-1} (x_{p,c} - \mu_{i,c}) \right) \tag{3}$$

where $x_{p,c}$ is a three-dimensional vector on the RGB values of pixel p, and for the colour image, $n = 3$ is the dimensionality. The dark channel is calculated following the formula as follows:

$$I_{\Omega_i}^{\mathrm{dark-sp}} = \min_{c \in \{r,g,b\}} \left(\min_{p \in \Omega_i \ and \ S_p > \mathrm{r}} (I^c(p)) \right) \tag{4}$$

where r is a constant. A large value of r may increase the transmission map and darken the restored image, while a small value of r cannot eliminate the block effect. We define r as 10^{-2} in our experiment; this value is suitable for most images we tested and can be adjusted to a value in $[10^{-3}, 10^{-1}]$ (Fig. 3). To avoid non-results, we establish the rule that if more than half of the pixels p in superpixel Ω_i cannot satisfy the constraint $S_p > r$, then we calculate the dark channel of superpixel Ω_i as follows:

$$I_{\Omega_i}^{\mathrm{dark-sp}} = \min_{c \in \{r,g,b\}} \left(\mathrm{median}_{p \in \Omega_i}(I^c(p)) \right) \tag{5}$$

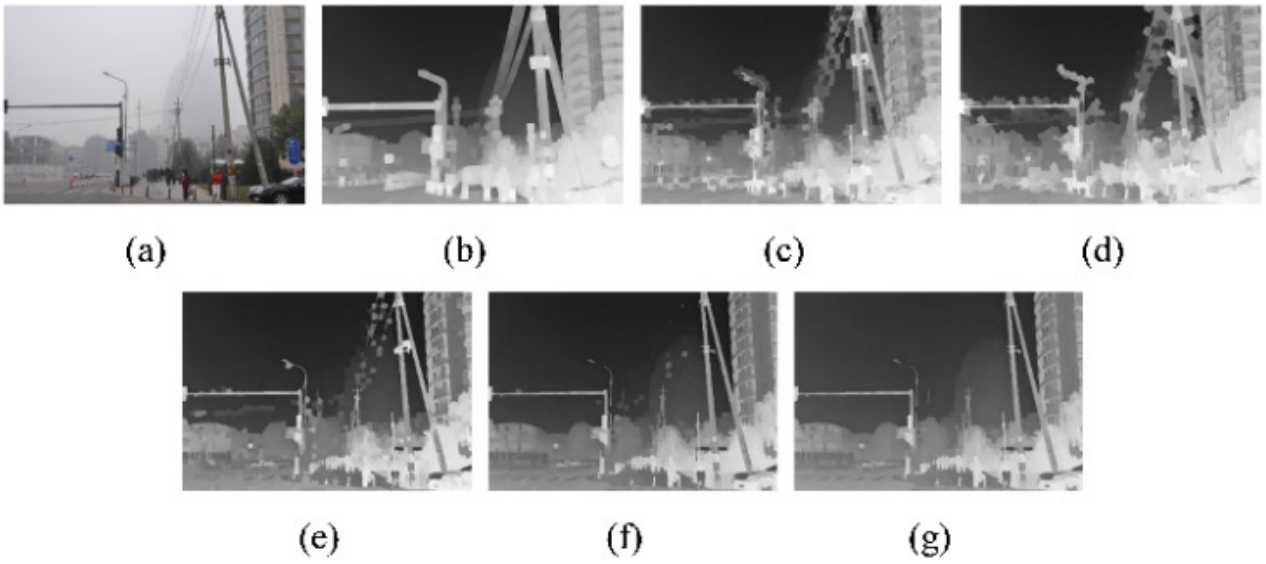

FIGURE 3. (a) Input image. (b-g) corresponding transmission maps obtained directly on windows or superpixels without any refinement (i.e., through guided filtering). There are always 2000 superpixels. (b) He's method (c) Yang's method. (d) Noh's method. (e-g) The proposed method with different values for the parameter: (e) r=10^{-5}, (f) r=10^{-2}, and (g) r=10^{-1}.

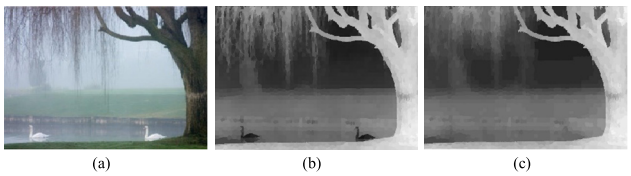

FIGURE 4. (a) Input image. (b) Corresponding initial transmission map obtained based on superpixels. (c) Corresponding revised transmission map from the superpixel-based MRF method. The error transmittance estimate for the geese in the initial transmission map is revised.

The superpixel-based transmission map is calculated by

$$t = 1 - \omega_1 \cdot I_{\Omega_i}^{\text{dark}-\text{sp}} \tag{6}$$

where ω_1 is a constant to keep a very small amount of haze. When $\omega_1 = 1$, the fog is completely removed, while a small value of ω_1 means that more fog will be retained. Similar to He's method [12], we let $\omega_1 = 0.9$ to achieve a better visual effect. A variable in our algorithm is the number of superpixels. On the one hand, superpixel boundaries and actual structural boundaries become incompatible for a small number of superpixels. On the other hand, if the number of superpixels is too large, the running time will become quite long. The number of superpixels is set to 3000 in our experiments.

B. REVISION OF TRANSMISSION MAP USING SUPERPIXELS AND MRF

The dehazing results recovered by the initial transmission map have better preserved structural edges. However, there is still an exception when there are objects with colours similar to that of light. This situation is challenging for the existing image dehazing algorithms (see the transmittance of the geese in Fig. 4). Moreover, neighbouring superpixels that are not on structural boundaries, always have similar scene depths and transmittances. For this reason, we refer to the idea of MRF.

The revised transmission map can be calculated by minimizing the energy function as follows:

$$E\left(\hat{t}\right) = \sum_{i} E(t_i, \hat{t}_i) + \sum_{i,j} N(t_i, t_j) \cdot E(\hat{t}_i, \hat{t}_j) \tag{7}$$

where t_i is the initial transmittance of superpixel i and $\hat{t}$ is the estimated revised transmittance. The data term $E(t_i, \hat{t}_i)$ represents the probability of superpixel i having a transmittance $\hat{t}_i$. The neighbour term $N(t_i, t_j)$ represents theintensity of the relevance between superpixels i and j. Thesmooth term $E(\hat{t}_i, \hat{t}_j)$ encodes the probability that neighbouring pixels have similar transmittance.

The data term should enhance the possibility of correcting the incorrectly estimated transmittance, which is usually statistically significantly different from its correctly estimated transmittance, while keeping the remaining values of superpixels as constant as possible. Thus, we characterize the data function in the following form:

$$E\left(t_i, \hat{t}_i\right) = \omega \cdot \log\left(\left|t_i - \hat{t}_i\right| + 1\right) \tag{8}$$

where ω is the weighing parameter, which is used to control the balance between the data term and smooth term. A large value of ω means that the estimated transmission map will be close to the initial transmission map, while a small value of ω means that the estimated results will be smoothed. The influence of ω on the estimated results can be seen in Fig. 7. Meanwhile, the form of the data term ensures that MRF does not produce halo effect on the edges, which enables the MRF to achieve a good boundary preservation effect.

The choice of the neighbour term $N(t_i, t_j)$ is a critical issue for edge preservation. Our method contains a structural edge

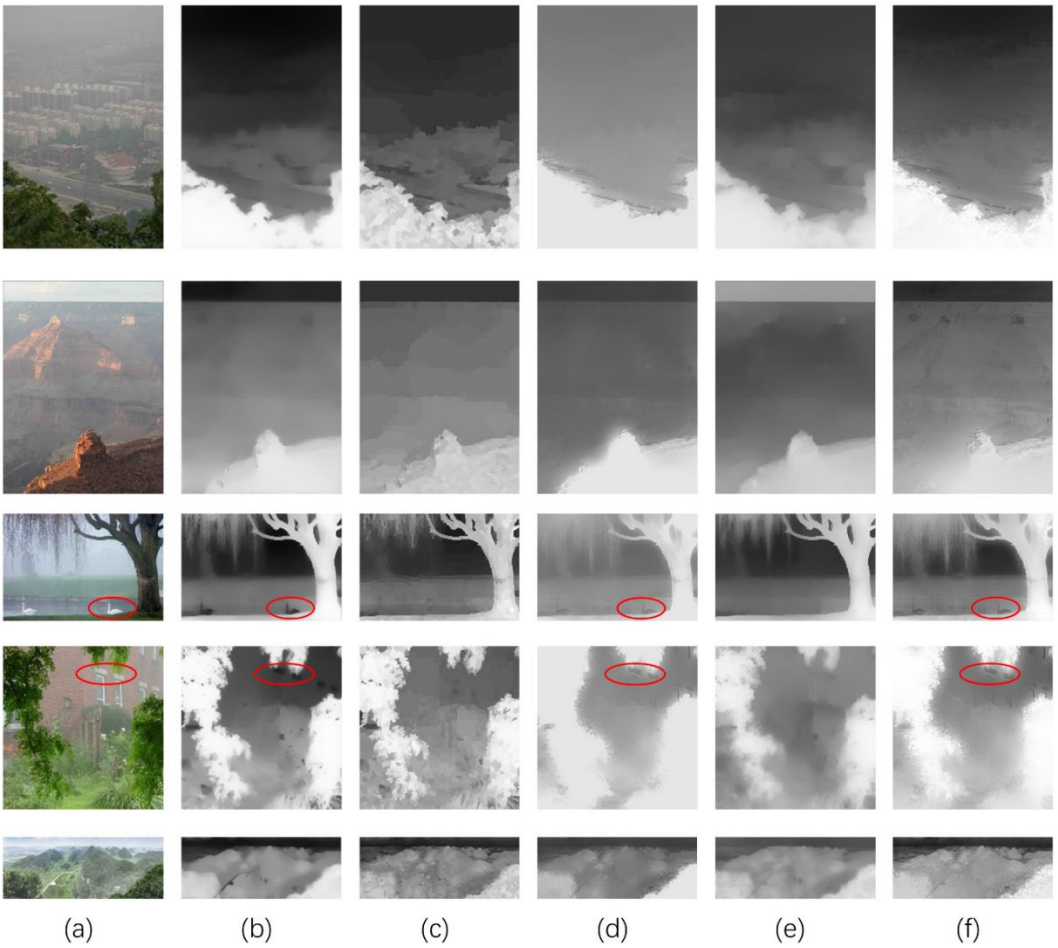

FIGURE 5. Comparisons of the transmission map estimation accuracies. (a) Input image. (b-f) Transmission maps obtained by (b) Meng's method, (c) the proposed method, (d) Zhu's method, (e) Berman's method and (f) He's method.

term, which is a general superpixelwise squared difference of transmittance, written as

$$S\left(t_i\right) = \sum_j g_{i,j} \cdot t_i \cdot \left|t_j - t_i\right|, \quad j \in \mathrm{R}_i \tag{9}$$

where j belongs to R_i, the circular region centred at the centre of superpixel i. $S\left(t_i\right)$ represents the spatial squared difference within region R_i. $g_{i,j}$ is a weighing function defined according to spatial affinity, expressed as

$$g_{i,j} \propto \exp\left(-\frac{\left(x_i - x_j\right)^2 + \left(y_i - y_j\right)^2}{2\sigma^2}\right) \tag{10}$$

where σ controls the spatial scale of the circular region. A small value of $S(t_i)$ indicates that superpixel i has great relevance with nearby superpixels and should be smoothed, while a large value denotes the possible structural edges (see Fig. 6 and Fig. 7). As can be seen in the figures, the designed structural edge term faithfully adheres to the edges. The neighbour term is characterized by the following:

$$N\left(t_i, t_j\right) = \begin{cases} \dfrac{1}{S\left(t_i\right) \cdot S\left(t_j\right) + \varepsilon}, & \text{if } j \in \mathrm{R}_i \\ 0, & \text{else} \end{cases} \tag{11}$$

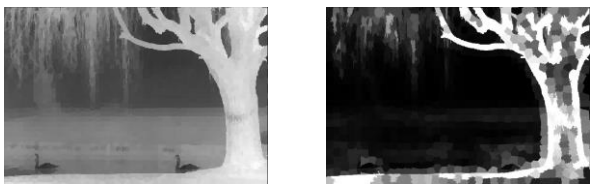

FIGURE 6. (a) Initial transmission map (the transmittance of the geese is incorrectly estimated). (b) $S(t)$, which represents the superpixels at possible structural edges.

where ε is a small constant to prevent the denominator from being 0, and its value is selected as 10^{-6}. This design of the neighbour term ensures that the structural edges are maintained.

The smooth function $E(\hat{t}_i, \hat{t}_j)$ encodes the probability that neighbouring superpixels have a similar depth. Generally, applying traditional smoothing functions such as $(\hat{t}_i - \hat{t}_j)^2$ may yield discontinuities of the structural edges and produce halo artefacts near boundaries [19], [20]. However, the neighbour term we introduced solves the boundary problem well. We characterize the smoothing term in the following form:

$$E\left(\hat{t}_i, \hat{t}_j\right) = \left|\hat{t}_i - \hat{t}_j\right| \tag{12}$$

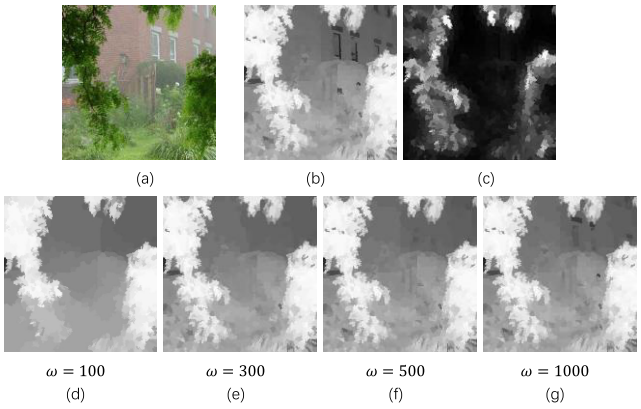

FIGURE 7. (a) Input image. (b) Initial transmission map obtained based on superpixels. (c) $S(t)$, which represents the superpixels at possible structural edges. (d-g) Revised transmission map based on superpixels and MRF with different values of weight coefficient ω.

To minimize the cost function of (7), we apply the graph cut technique [21] and employ the α-expansion algorithm [21] to solve the graph cut problem with good computational performance.

We analyse the accuracy of transmission map estimation through nonreference subjective assessment. As shown in Fig. 5, we compared the transmission maps captured by Meng's [22], Zhu's [13], Berman's [32], and He's methods [12] and the proposed method. The scene in the red circle is the nearby white object, whose transmittance is often misestimated. Meng's, Zhu's and He's methods fail to avoid this problem, while Berman's method and the proposed method perform well. However, the transmittance estimation of Berman's method at rapidly changing edges (see the estimated transmittance around the leaves on the trees in Fig. 5) is fuzzy, which will cause a halo effect.

C. RECOVERY OF THE SCENE RADIANCE

We pick the top 0.1% of the brightest pixels in the dark channel of the input image. These pixels are most hazy/opaque. The ambient light A_c is estimated to be the average of these pixels in the three colour channels. The scene radiance is recovered as

$$J_c(x) = \frac{I_c(x) - A_c}{\max(t(x), t_0)} + A_c \tag{13}$$

where $t_0 = 0.1$ prevents noise amplification when $t(x)$ is close to zero.

III. EXPERIMENTAL RESULTS

To assess the performance of the proposed method, we test it on various haze images and compare it with Meng's [22], Zhu's[13], Tarel's [11], He's [12], Berman's[32], and Codruta's [33] methods. For a fair comparison, we use the 7×7 patch in Meng's and He's methods. All the compared methods apply a lower bound of $t_0 = 0.1$ for the transmittance in (12) and a guided filter with the same parameters to smooth the transmission map.

A. QUALITIVE COMPARISON OF REAL-WORLD IMAGES

For the visual comparisons, we select 30 real-world outdoor images, which have rich edge information and a large range for the depth of field, and they are often used for contrast in research papers. By adopting Meng's [22], Zhu's [13], Tarel's [11], He's [12], Berman's [32], and Codruta's [33] methods and the proposed method, some of the restored images are shown in Fig. 10 for no-reference subjective qualitative comparisons. The contrast and visibility of the restored images are greatly improved compared with the original images. Nevertheless, the degrees of restoration are different. In the first row of Fig. 10, the red squares are the close-ups of the details; note that the degree of dehazing on the road is too low in the results of Zhu's, Berman's and He's methods, whereas Tarel's method realizes overly strong dehazing and its restored image is accompanied by colour distortions. Relative to the above methods, Codruta's and Meng's methods and the proposed method can achieve better results in reducing the halo effect among the structural boundaries. Meng's results in the close-shot scenery are close to those obtained by the proposed method, as displayed in Fig. 10. However, the effect of Meng's algorithm on long-shot scenery is oversaturated, especially the sky region, whereas the fog removal ability for Zhu's and Codruta's methods over distant scenes is weak.

Compared with the images restored by the compared algorithms, the images restored by our method have better sharpness, contrast and are free of oversaturation.

To evaluate the proposed method quantitatively, we apply a blind assessment metric [34] dedicated to visibility restoration to measure the haze removal effect. The input images and the restored results are transformed into greyscale images, which are used to calculate three indicators to evaluate the restoration effect. The number of edges that are newly visible after dehazing is denoted by indicator e. The mean of the ratio of the gradient norms over these edges both before and after restoration is denoted by indicator r. The percentage of pixels that become completely black or completely white after dehazing is denoted by indicator σ. Larger values of e and r and smaller values of σ indicate a better restoration effect. To analyse the results, the gradient images of edges are shown in Fig. 8. The images of (b), (c) and (g) are influenced by noise, which demonstrates Codruta's, Meng's and Berman's method have amplified the noise level while trying to improve the visibility of foggy images. The gradient images show that the proposed and He's methods perform better.

All 30 real-world outdoor images are restored by all the compared methods, the mean values of the three blind assessment indicators are calculated in Fig. 11, and Table. 1 shows the blind assessment results for restored images in Fig. 10. Fig. 11 and Table. 1 indicate that the proposed method outperforms the other methods in terms of the edge restoration and haze removal effects.

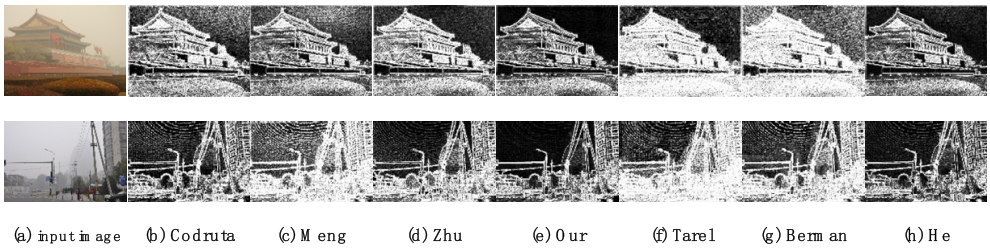

FIGURE 8. Gradients of results from different methods.

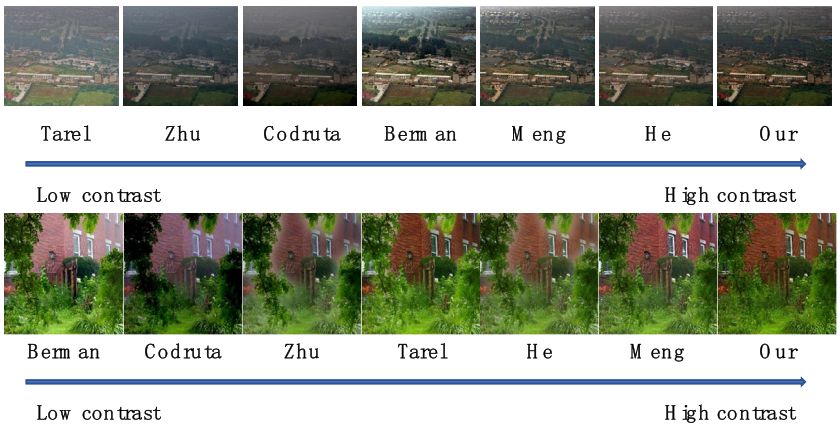

FIGURE 9. Evaluation of the final results by CEM.

TABLE 1. Evaluation results by the method proposed in [34].

Indicate	Results in Fig. 10	Codruta	Meng	Zhu	Our	Tarel	Berman	He
e	Row 1	1.316	1.583	0.816	1.334	**1.727**	1.284	1.319
	Row 2	3.493	4.930	2.701	**5.983**	3.090	5.239	3.591
	Row 3	0.004	0.386	0.211	**0.578**	0.391	0.577	0.282
	Row 4	0.227	**0.532**	0.237	0.400	0.449	0.520	0.225
	Row 5	0.276	0.619	0.392	**0.686**	0.644	0.684	0.531
	Row 6	1.773	2.210	1.167	2.797	2.165	**2.856**	2.145
Indicate	Results in Fig. 10	Codruta	Meng	Zhu	Our	Tarel	Berman	He
r	Row 1	2.022	3.046	1.482	**3.851**	3.413	3.246	2.251
	Row 2	1.929	3.677	1.766	**5.243**	2.989	4.760	2.421
	Row 3	1.324	1.927	1.202	**2.988**	2.216	2.264	1.338
	Row 4	0.573	1.775	1.218	1.950	2.192	**1.995**	1.201
	Row 5	0.885	1.636	1.280	**2.477**	1.992	2.193	1.359
	Row 6	0.875	1.825	1.362	2.996	3.001	**3.012**	1.368
Indicate	Results in Fig. 10	Codruta	Meng	Zhu	Our	Tarel	Berman	He
σ	Row 1	**0.000**	0.002	**0.000**	0.037	**0.000**	0.092	**0.000**
	Row 2	0.259	**0.000**	**0.000**	0.086	**0.000**	0.003	**0.000**
	Row 3	17.774	0.005	0.213	0.343	0.001	0.778	**0.000**
	Row 4	0.440	0.284	0.965	0.256	0.001	1.317	0.032
	Row 5	**0.000**	**0.000**	0.046	**0.000**	**0.000**	0.011	**0.000**
	Row 6	0.015	0.003	31.441	0.025	**0.000**	0.090	0.001

A perceptual evaluation using the contrast enhancement metric (CEM) was carried out, and improved by machine learning [44]. CEM has a good correlation with human judgments and sort images by their contrast. Fig. 9 presents the CEM of our and the compared results. Then we rank their performance according to CEM. The CEM is also trained with human's intuition. As a result, the CEM evaluation shows the proposed method outperforms the others.

B. QUALITATIVE COMPARISON OF SYNTHESIZED IMAGES

The first step is to synthesize foggy images for evaluation. The ground truth images, and their corresponding ground truth depth maps are chosen from the Middlebury Stereo datasets [23]–[25]. The synthesized images can be obtained by

$$J = I \cdot \mathrm{e}^{-\beta \cdot d} + A \cdot \left(1 - \mathrm{e}^{-\beta \cdot d}\right) \tag{14}$$

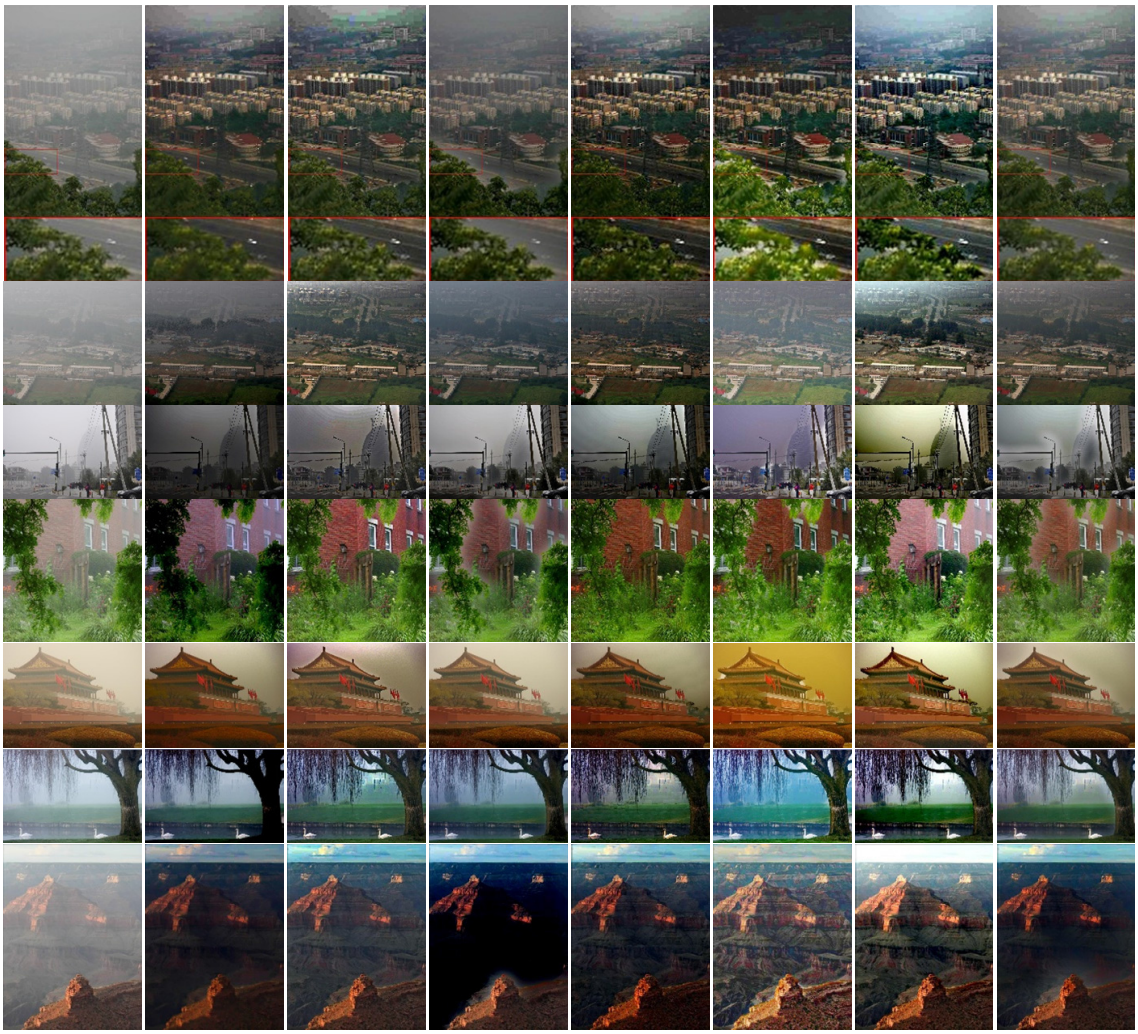

FIGURE 10. Qualitative comparison of the different methods on real-world images. (a) The hazy images. (b) Codruta's [33] results. (c) Meng's [22] results. (d) Zhu's [13] results. (e) Our results. (f) Tarel's [11] results. (g) Berman's [32] results. (h) He's [12] results.

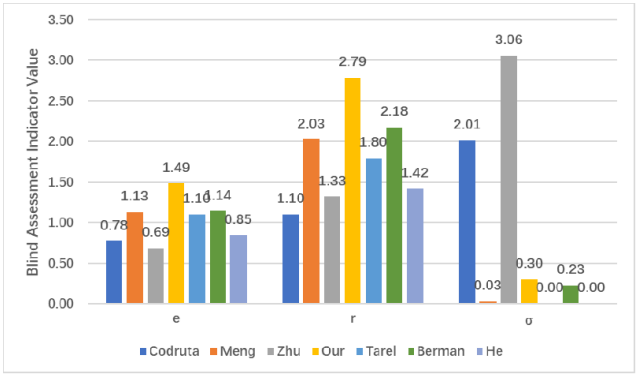

FIGURE 11. Averaged blind assessment indicators (e, r, σ) of the compared algorithms.

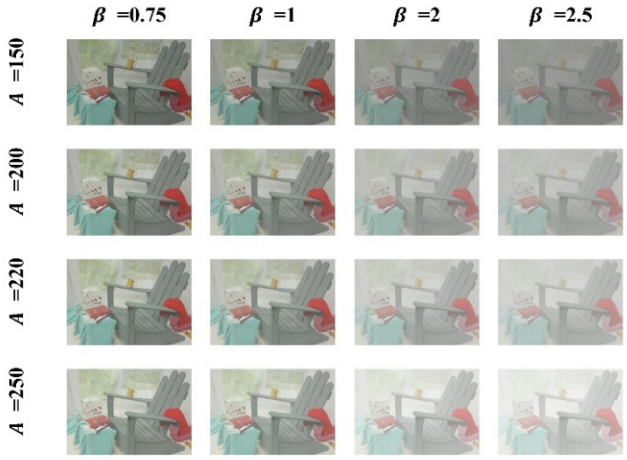

FIGURE 12. A group of synthesized 'Adirondack' images with different background light values A and attenuation coefficients β.

where d is the depth map obtained directly from the datasets. The background light A takes values in the set {150, 200, 220, 250} for testing. The attenuation coefficient β takes values in the set {0.75, 1, 2, 2.5} for simulating different turbidities.

All the compared algorithms are tested on the synthesized images with different A and β vaues. Fig. 12 shows a group of synthesized images.

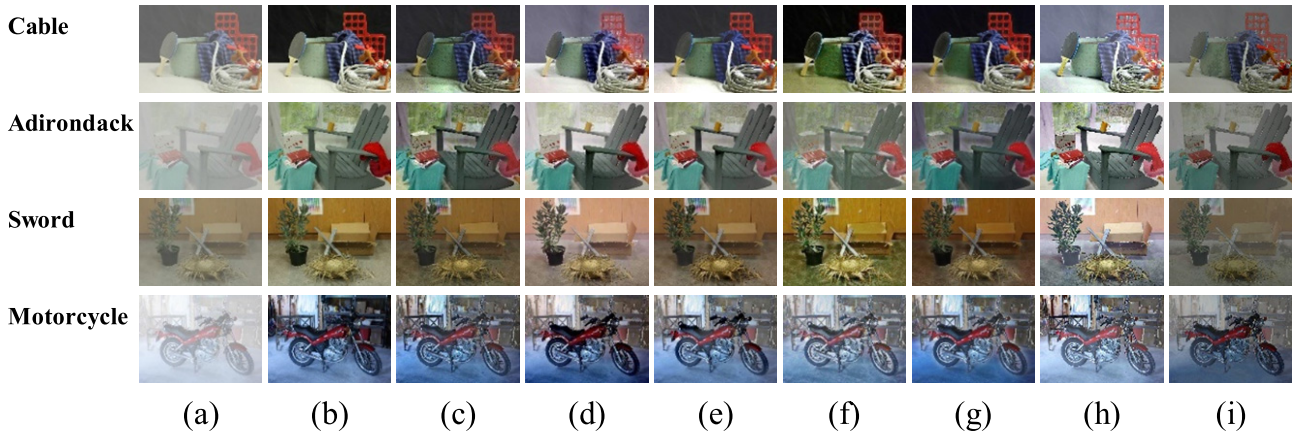

FIGURE 13. Restoration of the synthesized images. (a) Hazy images. (b) Ground truth images. (c) Meng's [22] results. (d) Zhu's [13] results. (e) Our results. (f) Tarel's [11] results. (g) He's [12] results. (h) Berman's [32] results. (i) Codruta's [33] results.

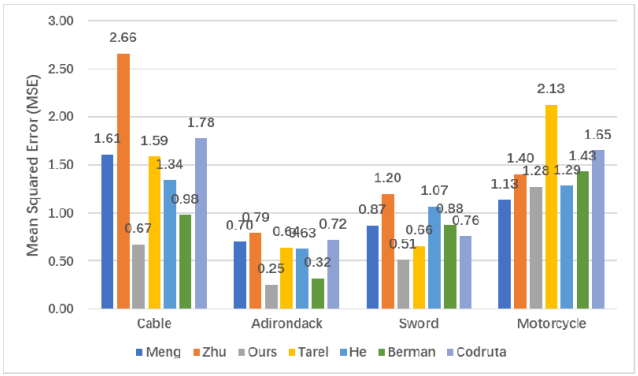

FIGURE 14. Average MSEs of all the compared algorithms.

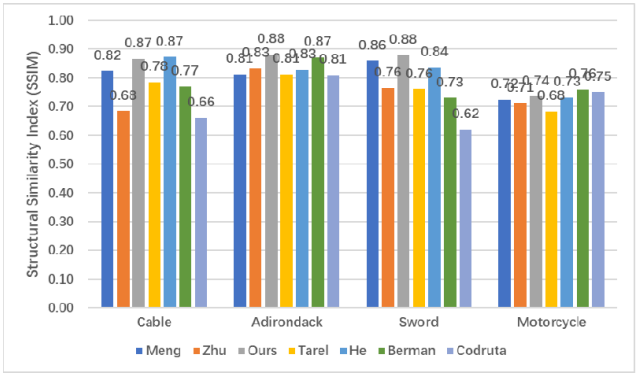

FIGURE 15. Average SSIMs of all the compared algorithms.

Fig. 13 shows some of the images restored by the compared methods. We compute the MSE and SSIM results to assess the performance of all the compared methods. A low MSE indicates that the restored image is close to the ground truth image, while a high SSIM represents a strong ability to preserve the structural information. The results shown in Fig. 14 and Fig. 15 are the average MSEs and SSIMs for each of the ground truth images with their 16 synthesized images. As seen, the weak defogging ability over distant scenes of Codruta's and Zhu's methods yields the highest MSEs and lowest SSIMs overall. The average MSEs and SSIMs of Berman's and He's results are better than Meng's and Tarel's results, which usually suffer from overenhancement. In contrast, our method achieves the best value over all the test modes, which indicates that our method has better colour fidelity and preserves structural boundaries better than the other methods.

IV. CONCLUSION

In this paper, we propose a novel image dehazing algorithm using an MRF on the superpixel domain. By means of superpixels, the block effect and halo artefacts can be avoided. Moreover, underestimating the transmittance in the area where pixel colour is close to that of light is avoidable by utilizing an MRF. The restored results show that the proposed method can achieve better results than other state-of-the-art image dehazing methods under different turbidity and lighting conditions.

REFERENCES

[1] S. G. Narasimhan and S. K. Nayar, "Chromatic framework for vision in bad weather," in *Proc. IEEE Conf. Comput. Vis. Pattern Recognit. (CVPR)*, Hilton Head Island, SC, USA, Jun. 2000, pp. 598–605.
[2] S. K. Nayar and S. G. Narasimhan, "Vision in bad weather," in *Proc. 7th IEEE Int. Conf. Comput. Vis.*, Kerkyra, Greece, Sep. 1999, pp. 820–827.
[3] S. G. Narasimhan and S. K. Nayar, "Contrast restoration of weather degraded images," *IEEE Trans. Pattern Anal. Mach. Intell.*, vol. 25, no. 6, pp. 713–724, Jun. 2003.
[4] Y. Y. Schechner, S. G. Narasimhan, and S. K. Nayar, "Instant dehazing of images using polarization," in *Proc. IEEE Comput. Soc. Conf. Comput. Vis. Pattern Recognit. (CVPR)*, Kauai, HI, USA, Dec. 2001, pp. 325–332.
[5] S. Shwartz, E. Namer, and Y. Y. Schechner, "Blind haze separation," in *Proc. IEEE Comput. Soc. Conf. Comput. Vis. Pattern Recognit. (CVPR)*, New York, NY, USA, vol. 2, Jun. 2006, pp. 1984–1991.
[6] S. G. Narasimhan, Y. Y. Schechner, and S. K. Nayar, "Polarization-based vision through haze," *Appl. Opt.*, vol. 42, no. 3, pp. 511–525, Jan. 2003.
[7] S. G. Narasimhan and S. K. Nayar, "Vision and the atmosphere," *Int. J. Comput. Vis.*, vol. 48, no. 3, pp. 233–254, 2002.
[8] T. Treibitz and Y. Y. Schechner, "Active polarization descattering," *IEEE Trans. Pattern Anal. Mach. Intell.*, vol. 31, no. 3, pp. 385–399, Mar. 2009.
[9] R. T. Tan, "Visibility in bad weather from a single image," in *Proc. IEEE Conf. Comput. Vis. Pattern Recognit.*, Anchorage, AK, USA, Jun. 2008, pp. 1–8.
[10] R. Fattal, "Single image dehazing," *ACM Trans. Graph.*, vol. 27, no. 3, pp. 1–9, Aug. 2008.

[11] J.-P. Tarel and N. Hautiere, "Fast visibility restoration from a single color or gray level image," in *Proc. IEEE 12th Int. Conf. Comput. Vis.*, Kyoto, ON, USA, Sep. 2009, pp. 2201–2208.
[12] K. He, J. Sun, and X. Tang, "Single image haze removal using dark channel prior," *IEEE Trans. Pattern Anal. Mach. Intell.*, vol. 33, no. 12, pp. 2341–2353, Dec. 2011.
[13] Q. Zhu, J. Mai, and L. Shao, "A fast single image haze removal algorithm using color attenuation prior," *IEEE Trans. Image Process.*, vol. 24, no. 11, pp. 3522–3533, Nov. 2015.
[14] W. Wang, X. Yuan, X. Wu, and Y. Liu, "Fast image dehazing method based on linear transformation," *IEEE Trans. Multimedia*, vol. 19, no. 6, pp. 1142–1155, Jun. 2017.
[15] S.-L. Wong, Y.-P. Yu, N. A.-J. Ho, and R. Paramesran, "Comparative analysis of underwater image enhancement methods in different color spaces," in *Proc. Int. Symp. Intell. Signal Process. Commun. Syst. (ISPACS)*, Kuching, Malaysia, Dec. 2014, pp. 034–038.
[16] R. Achanta, A. Shaji, K. Smith, A. Lucchi, P. Fua, and S. Süsstrunk, "SLIC superpixels compared to state-of-the-art superpixel methods," *IEEE Trans. Pattern Anal. Mach. Intell.*, vol. 34, no. 11, pp. 2274–2281, Nov. 2012.
[17] M. Yang, Z. Li, and J. Liu, "Super-pixel based single image haze removal," in *Proc. Chin. Control Decis. Conf. (CCDC)*, Yinchuan, China, May 2016, pp. 1965–1969.
[18] S.-W. Noh, B. Ahn, and I. S. Kweon, "Haze removal on superpixel domain," in *Proc. 10th Int. Conf. Ubiquitous Robots Ambient Intell. (URAI)*, Jeju, South Korea, Oct. 2013, pp. 597–598.
[19] J. Besag, "On the statistical analysis of dirty pictures," *J. Roy. Stat. Soc. B, Methodol.*, vol. 48, no. 3, pp. 259–279, Jul. 1986.
[20] Y. Boykov, O. Veksler, and R. Zabih, "Fast approximate energy minimization via graph cuts," *IEEE Trans. Pattern Anal. Mach. Intell.*, vol. 23, no. 11, pp. 1222–1239, Nov. 2001.
[21] A. Delong, A. Osokin, H. N. Isack, and Y. Boykov, "Fast approximate energy minimization with label costs," in *Proc. IEEE Comput. Soc. Conf. Comput. Vis. Pattern Recognit.*, San Francisco, CA, USA, 2010, pp. 2173–2180.
[22] G. Meng, Y. Wang, J. Duan, S. Xiang, and C. Pan, "Efficient image dehazing with boundary constraint and contextual regularization," in *Proc. IEEE Int. Conf. Comput. Vis.*, Sydney, NSW, Australia, Dec. 2013, pp. 617–624.
[23] D. Scharstein and R. Szeliski, "A taxonomy and evaluation of dense two-frame stereo correspondence algorithms," *Int. J. Comput. Vis.*, vol. 47, no. 1, pp. 7–42, Apr. 2002.
[24] D. Scharstein and R. Szeliski, "High-accuracy stereo depth maps using structured light," in *Proc. IEEE Comput. Soc. Conf. Comput. Vis. Pattern Recognit.*, Madison, WI, USA, Jun. 2003, pp. 195–202.
[25] D. Scharstein, H. Hirschmüller, Y. Kitajima, G. Krathwohl, N. Nešić, X. Wang, and P. Westling, "High-resolution stereo datasets with subpixel-accurate ground truth," in *Proc. German Conf. Pattern Recognit. (GCPR)*, Münster, Germany, 2014, pp. 31–42.
[26] K. He, J. Sun, and X. Tang, "Guided image filtering," *IEEE Trans. Pattern Anal. Mach. Intell.*, vol. 35, no. 6, pp. 1397–1409, Jun. 2013.
[27] Z. Li, J. Xie, D. Tu, and Y.-J. Choi, "Sparse signal recovery by stepwise subspace pursuit in compressed sensing," *Int. J. Distrib. Sensor Netw.*, vol. 9, no. 8, Aug. 2013, Art. no. 798537.
[28] Z. Li, Y. Xie, Y. Choi, G. Zhu, X. Peng, and J. Xie, "Block-based projection matrix design for compressed sensing," *Chin. J. Electron.*, vol. 25, no. 3, pp. 551–555, May 2016.
[29] E. H. Land and J. J. McCann, "Lightness and retinex theory," *J. Opt. Soc. Amer. A, Opt. Image Sci.*, vol. 61, no. 1, pp. 1–11, 1971.
[30] E. H. Land, "Recent advances in retinex theory," *Vis. Res.*, vol. 26, no. 1, pp. 7–21, Jan. 1986.
[31] J. Wang, K. Lu, J. Xue, N. He, and L. Shao, "Single image dehazing based on the physical model and MSRCR algorithm," *IEEE Trans. Circuits Syst. Video Technol.*, vol. 28, no. 9, pp. 2190–2199, Sep. 2018.
[32] D. Berman, T. Treibitz, and S. Avidan, "Non-local image dehazing," in *Proc. IEEE Conf. Comput. Vis. Pattern Recognit. (CVPR)*, Las Vegas, NV, USA, Jun. 2016, pp. 1674–1682.
[33] C. O. Ancuti and C. Ancuti, "Single image dehazing by multi-scale fusion," *IEEE Trans. Image Process.*, vol. 22, no. 8, pp. 3271–3282, Aug. 2013.
[34] N. Hautiere, J. P. Tarel, D. Aubert, and E. Dumont, "Blind contrast enhancement assessment by gradient ratioing at visible edges," *Image Anal. Stereology*, vol. 27, no. 2, pp. 87–95, 2008.
[35] D. Singh, V. Kumar, and M. Kaur, "Single image dehazing using gradient channel prior," *Int. J. Speech Technol.*, vol. 49, no. 12, pp. 4276–4293, Dec. 2019.
[36] D. Singh and V. Kumar, "Dehazing of remote sensing images using fourth-order partial differential equations based trilateral filter," *IET Comput. Vis.*, vol. 12, no. 2, pp. 208–219, Mar. 2018.
[37] D. Singh and V. Kumar, "Single image haze removal using integrated dark and bright channel prior," *Modern Phys. Lett. B*, vol. 32, no. 4, Feb. 2018, Art. no. 1850051.
[38] D. Singh and V. Kumar, "Defogging of road images using gain coefficient-based trilateral filter," *J. Electron. Imag.*, vol. 27, Jan. 2018, Art. no. 013004.
[39] D. Singh and V. Kumar, "Modified gain intervention filter based dehazing technique," *J. Modern Opt.*, vol. 64, no. 20, pp. 2165–2178, Nov. 2017.
[40] D. Singh and V. Kumar, "Dehazing of remote sensing images using improved restoration model based dark channel prior," *Imag. Sci. J.*, vol. 65, no. 5, pp. 282–292, Jul. 2017.
[41] W. Wang, A. Wang, Q. Ai, C. Liu, and J. Liu, "AAGAN: Enhanced single image dehazing with attention-to-attention generative adversarial network," *IEEE Access*, vol. 7, pp. 173485–173498, 2019.
[42] L. Shen, Y. Zhao, Q. Peng, J. C.-W. Chan, and S. G. Kong, "An iterative image dehazing method with polarization," *IEEE Trans. Multimedia*, vol. 21, no. 5, pp. 1093–1107, May 2019.
[43] Q. Wu, W. Ren, and X. Cao, "Learning interleaved cascade of shrinkage fields for joint image dehazing and denoising," *IEEE Trans. Image Process.*, vol. 29, pp. 1788–1801, Sep. 2019.
[44] K. B. Gibson and T. Q. Nguyen, "A no-reference perceptual based contrast enhancement metric for ocean scenes in fog," *IEEE Trans. Image Process.*, vol. 22, no. 10, pp. 3982–3993, Oct. 2013.

YIBO TAN received the B.Eng. degree from the Ocean University of China, in 2014, where he is currently pursuing the master's and Ph.D. degrees in intelligent information and communication systems. His research interests include image processing and computer vision.

GUOYU WANG received the B.S. and M.S. degrees in ocean physics from the Ocean College of Shandong, Qingdao, China, in 1984 and 1987, respectively, and the Ph.D. degree from the Faculty of Electrical Engineering, The Netherlands, in 2000. He is currently a Professor with the Ocean University of China. His research interests include pattern recognition and image processing and analysis.